Journal of Magnetic Resonance 198 (2009) 132–136

Contents lists available at ScienceDirect

Journal of Magnetic Resonance

journal homepage: www.elsevier.com/locate/jmr

Communication

Nuclear magnetic resonance in microfluidic environments using inductively coupled radiofrequency resonators

Marcel Utz [a,b,*], Reza Monazami [b]

[a] Center For Microsystems For The Life Sciences, University of Virginia, Charlottesville, VA 22904, USA
[b] Department of Mechanical and Aeropspace Engineering, University of Virginia, 122 Engineer's Way, Charlottesville, VA 22904, USA

ARTICLE INFO

Article history:
Received 11 November 2008
Revised 8 January 2009
Available online 30 January 2009

Keywords:
Inductive coupling
Microresonator
Sensitivity

ABSTRACT

Inductively coupled radiofrequency resonators can provide NMR signals from small samples wirelessly and with high sensitivity. We explore the achievable sensitivity depending on the resonator's *Q*-factor and its cross-inductance to the NMR probe. Even for small resonators with modest *Q*, the sensitivity can be close to that of directly (impedance) coupled microcoils. Sensitivity and excitation power inside inductively coupled solenoids were monitored experimentally by microimaging. The flow velocity profile inside a capillary of 200 μm diameter was measured with a resolution and sensitivity that rivals recent work based on directly coupled microcoils.

1. Introduction

Inductively coupled [1,2] radio frequency (rf) resonators inserted into the probe volume of a conventional nuclear magnetic resonance (NMR) spectrometer offer the possibility to focus the sensitivity and radio frequency power on small volumes. Providing a crucial advantage in situations where the available sample volume is limited, this has recently been exploited to boost sensitivity in magic angle spinning experiments [3]. Microfluidic devices could greatly benefit from this principle also, because it eliminates the need for electrical leads between the microfluidic system and the spectrometer. In the present contribution, the limits of achievable sensitivity are explored with respect to the parameters of the resonator. It is demonstrated that inductively coupled microcoils can rival the performance of directly connected ones, provided that inductive coupling is sufficiently strong.

To optimize sensitivity, the NMR receiver coil must tightly enclose the available sample volume. In the context of microfluidic devices, this requirement has been met by integrating planar coils directly into the chip [4–7], and by remote detection [8–10]. In the latter approach, the chip resides in a conventional gradient probe, inside a large rf coil which is used for excitation only. Nuclear precession is detected downstream by a microcoil wrapped around a capillary connected to the chip. In both cases, an active connection to the chip, either electrical or fluidic, is needed during the acquisition of NMR data. However, applications requiring mass throughput, for example medical diagnostic screening, would greatly benefit if it were possible to characterize the contents of the chip by NMR without the need for any connections. This can be accomplished by integrating tuned microresonators, into the chip, and coupling them *inductively* to the NMR system.

NMR data is usually obtained from the nuclear induction in a resonator tuned to the Larmor frequency [11–13]. The resonator is connected to a broadband preamplifier via a matched transmission line. The resulting mass sensitivity depends inversely on the coil volume [14–18]. A number of alternative detection schemes have been proposed (see, for example, [19–23]) but none of them has turned out to be as generally applicable as the nuclear induction method.

Wu et al. have used microcoils to obtain NMR spectra from an electrophoresis capillary with 75μm inner diameter [24]. Immersion of the microcoil in a susceptibility-matched medium provides high spectral resolution [25]. NMR spectra from lipid globules with a voxel volume as small as 5 pL have been obtained in this manner [26], and experimental techniques integrating liquid chromatography and capillary electrophoresis with NMR have been developed [27–32]. Recently, Zhang and Webb obtained detailed flow velocity field information in sub-mm size capillaries [33]. While these studies have all relied on resistive coupling of the microcoils, it is the goal of the present paper to show that *inductive*, wireless coupling offers similar performance.

To achieve this, a closed-loop resonator, usually composed of an inductor coil and a tuning capacitor, is inserted into a conventional NMR probe. The cross-inductance between the resonator coil and the probe leads to a focusing of both the rf intensity and the sensitivity to the volume enclosed by the resonator inductor. This field-focusing effect can be visualized directly by magnetic resonance imaging, as illustrated in Fig. 1A. It shows a slice

* Corresponding author. Fax: +1 434 924 7424.
E-mail address: mu3q@virginia.edu (M. Utz).

1090-7807/$ - see front matter © 2009 Elsevier Inc. All rights reserved.
doi:10.1016/j.jmr.2009.01.028

through a 1.5 mm ID solenoid coil tuned to the proton Larmor frequency by a parallel capacitor. The image has been obtained in an unmodified commercial microimaging probe, by inserting the resonator into an NMR tube filled with doped water. The water inside the coil gives a signal that is more than two orders of magnitude stronger than outside, due to the combined effect of the higher rf amplitude inside the solenoid and the enhanced sensitivity. In the remainder of this paper, this effect is treated quantitatively as a function of the cross-inductance and quality factor of the resonator, and it is shown that the Hagen-Poiseuille flow profile inside a capillary of 200 μm inner diameter can be measured using this principle with a sensitivity that is comparable to similar measurements carried out with directly connected microcoils [33].

2. Theory

A conceptual circuit diagram of an inductively coupled microresonator is shown in Fig. 2A. The microresonator is represented by an inductance L_μ and a capacitance C_μ, while the NMR probe circuit consists of the receiver coil L_T and the tuning (C_T) and matching (C_M) capacitors. The resistive losses in the probe and microresonator are represented by series resistances R_T and R_μ, respectively. The microresonator and the probe circuit are coupled through a mutual inductance $M_\mu = k\sqrt{L_\mu L_T}$, where $0 < k < 1$ is the coupling constant. For concentric solenoid coils, $k = \sqrt{V_\mu/V_T}$, where V_μ and V_T are the volumes of the micro- and probe coils, respectively. In the context of microfluidics, planar spiral coils are of particular interest [4–7]. In this case, the coupling constant can be estimated by adding the magnetic flux caused by the probe coil in each turn of the planar coil.

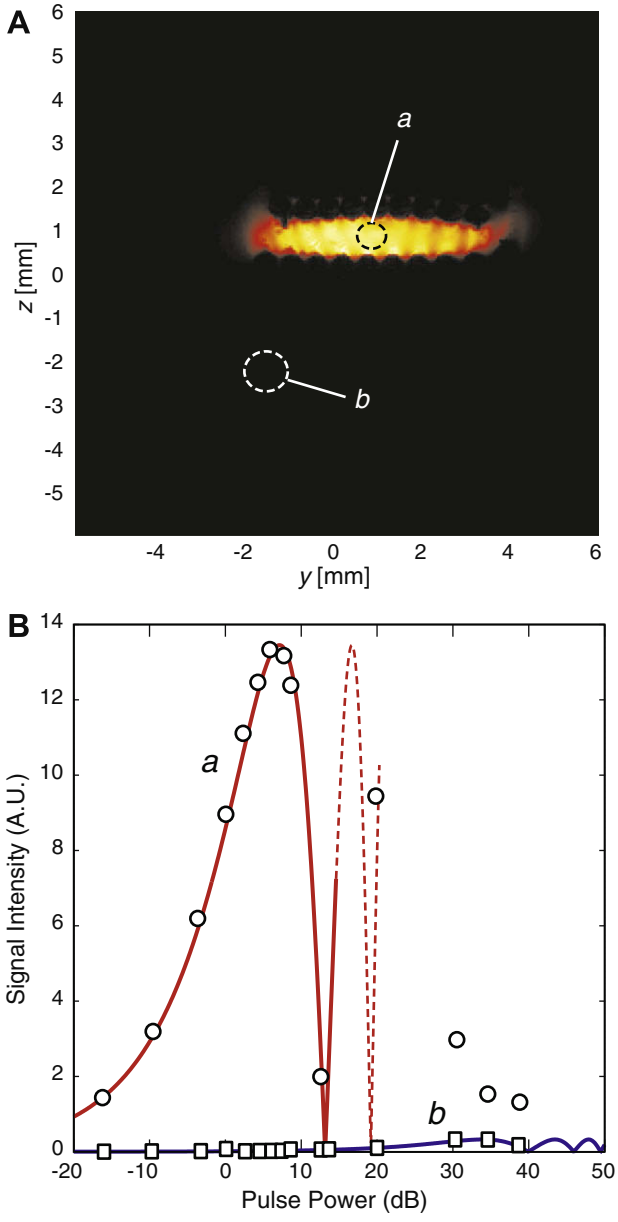

Fig. 1. (Color online) (A) NMR image of a tuned microcoil resonator immersed in doped water. Slice thickness is 0.2 mm. The volume inside the coil provides a very strong signal, whereas the surrounding water is all but invisible. (B) Absolute value of the signal amplitude inside (round symbols and red line (fit)) and outside (square symbols and blue line) of the tuned microcoil as a function of excitation pulse power. Data was acquired using a gradient-echo pulse sequence with a sinc-shaped excitation pulse of 2000 μs.

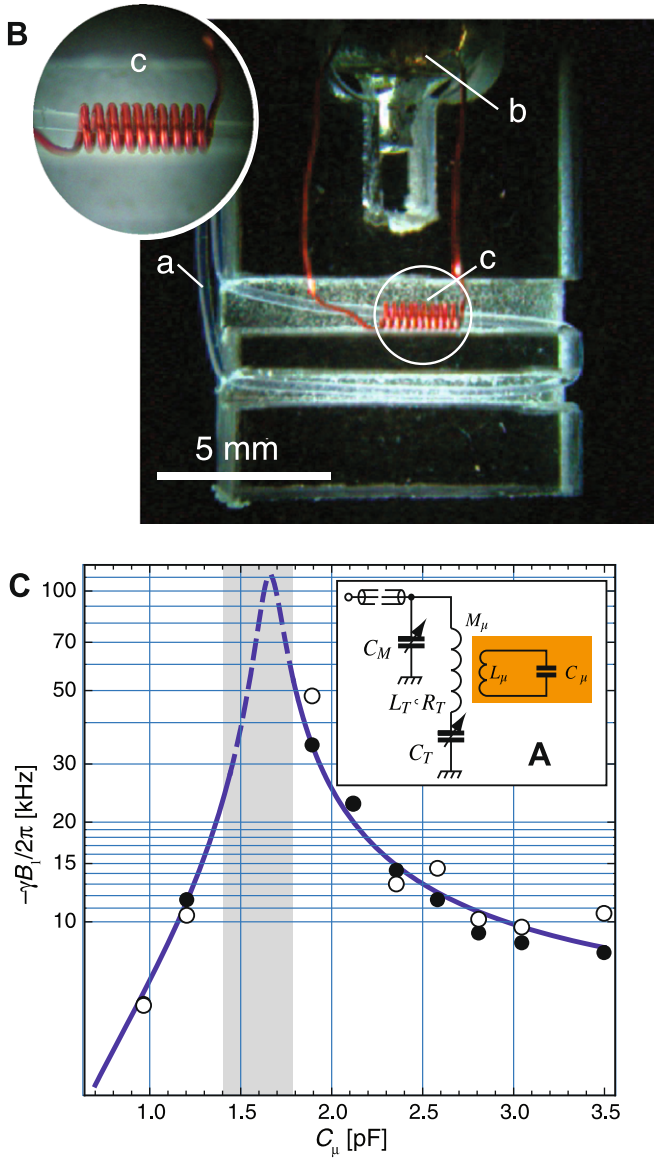

Fig. 2. (Color online) (A) Equivalent circuit diagram of an NMR probe circuit coupled to an rf microresonator. (B) Micrograph of a capillary (a) running through an rf resonator consisting of an adjustable capacitor (b) connected to a microcoil (c). (C) Signal amplitude (solid symbols, arbitrary units) and radio frequency field strength (open symbols, in units of proton nutation frequency), as a function of resonator capacitance C_μ in a microresonator composed of a 9 turn, 0.56 mm ID solenoid and a tunable capacitor.

According to the principle of reciprocity [15] the nuclear induction signal from a given number of spins is proportional to the rf field strength caused by a unit of current in the receiver coil. Analysis of the circuit in Fig. 2A yields for the total apparent impedance of the resonant part of the NMR probe (L_T combined with C_T)

$$Z_2 = R_T + i\omega L_T + \frac{1}{i\omega C_T} + \frac{\omega^2 k^2 L_\mu L_T}{R_\mu + i\omega L_\mu + 1/i\omega C_\mu}. \quad (1)$$

In the absence of coupling to a microresonator ($k = 0$), this describes a simple resonance, indicated, among other things, by a vanishing reactance if $\omega = \omega_0 = 1/\sqrt{L_T C_T}$. This is shown by the dashed line in Fig. 3. In the case of finite coupling to a tuned microresonator $\omega_0 = 1/\sqrt{L_T C_T} = 1/\sqrt{L_\mu C_\mu}$, the resonance persists, but is altered. For small values of k, the reactance exhibits a minor change in slope, whereas for larger k values, the slope is inverted and three distinct frequencies with vanishing reactance exist. In this latter case, the resonance is split into two peaks. It can be shown that the slope of the reactance at the resonance frequency is negative if $k > 1/Q_\mu$, where Q_μ is the quality factor of the microresonator. A split resonance means that the circuit must be designed such as to place one of the two resonance peaks at the Larmor frequency, and that neither the probe nor the mircoresonator is at resonance at that frequency by itself. For most practical cases, however, we anticipate that the effective coupling constant will be below this limit. For our further discussion, we may, therefore, assume that both the probe and the mircoresonator are tuned separately to the Larmor frequency. This substantially simplifies the following discussion. We have in this case

$$Z_2 = R_T + \frac{\omega^2 M_\mu^2}{R_\mu} = R_T(1 + k^2 Q_\mu Q_T), \quad (2)$$

where Q_μ and Q_T denote the quality factors of the microresonator and the probe circuit, respectively.

At resonance, the ratio of the current magnitudes in the microcoil and the probe coil is

$$\frac{I_\mu}{I_T} = \frac{\omega M_\mu}{R_\mu} = \omega \frac{k\sqrt{L_\mu L_T}}{R_\mu}. \quad (3)$$

In the absence of a microresonator, the direct induction in the receiver coil L_T is measured. In this case, the SNR is proportional to

$$(S/N)_{\text{probe}} \sim \frac{B_T}{I_T\sqrt{R_T}} \quad (4)$$

since the noise is proportional to $\sqrt{R_T}$. Similarly, if the microcoil is directly connected to an rf receiver, the signal/noise ratio is proportional to

$$(S/N)_{\text{direct}} \sim \frac{B_\mu}{I_\mu\sqrt{R_\mu}} \quad (5)$$

Finally, if the signal is observed in the probe coil, while it is coupled inductively to the microresonator, the SNR is

$$(S/N)_{\text{RF}} \sim \frac{B_\mu}{I_T\sqrt{R_T(1 + k^2 Q_\mu Q_T)}}, \quad (6)$$

where the factor $(1 + k^2 Q_\mu Q_T)$ accounts for the additional dissipation due to the microresonator. For solenoid coils, the sensitivity enhancement by the inductively coupled microresonator is found after some algebra as

$$\frac{(S/N)_{\text{RF}}}{(S/N)_{\text{probe}}} = Q_\mu \frac{k\sqrt{V_T/V_\mu}}{\sqrt{1 + k^2 Q_\mu Q_T}}. \quad (7)$$

The quality factor of the microresonator Q_μ provides an upper bound for this enhancement. In the present context, the alternatives of coupling the microcoil inductively, or observing the signal from it directly must be compared. In other words, is there a price to pay in sensitivity for the convenience of wireless coupling? The relevant sensitivity ratio is given by

$$\frac{(S/N)_{\text{RF}}}{(S/N)_{\text{direct}}} = \frac{k\sqrt{Q_\mu Q_T}}{\sqrt{1 + k^2 Q_\mu Q_T}}. \quad (8)$$

This relationship is plotted in Fig. 4 as a function of the Q-factor of the microresonator, assuming $Q_T = 200$, a typical value. The curves are parametrized with k^2, which corresponds to the volume ratio V_μ/V_T for solenoid coils. With $Q_T = 200$, Eq. (8) predicts that even

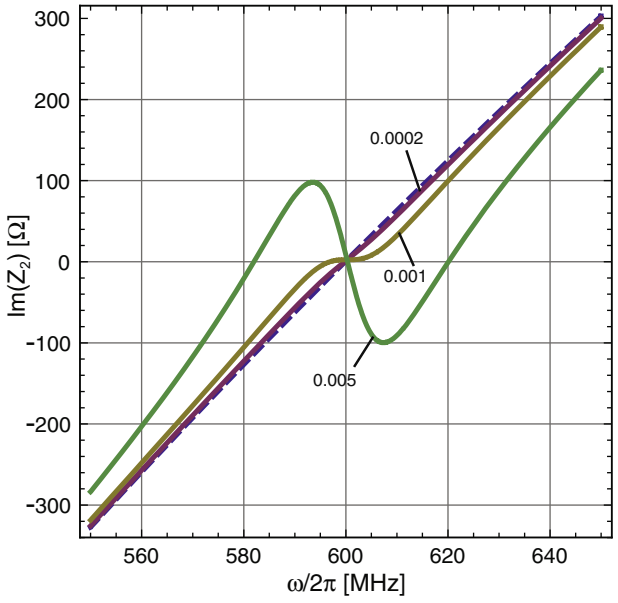

Fig. 3. Reactance (imaginary part of Z_2) of the circuit shown in Fig. 2A as a function of frequency, with both the probe and the resonator tuned to 600 MHz, using typical values for the inductances and capacitances. Dashed line: $k^2 = 0$; solid lines: $k^2 = 0.0002$, 0.001, and 0.005, as indicated.

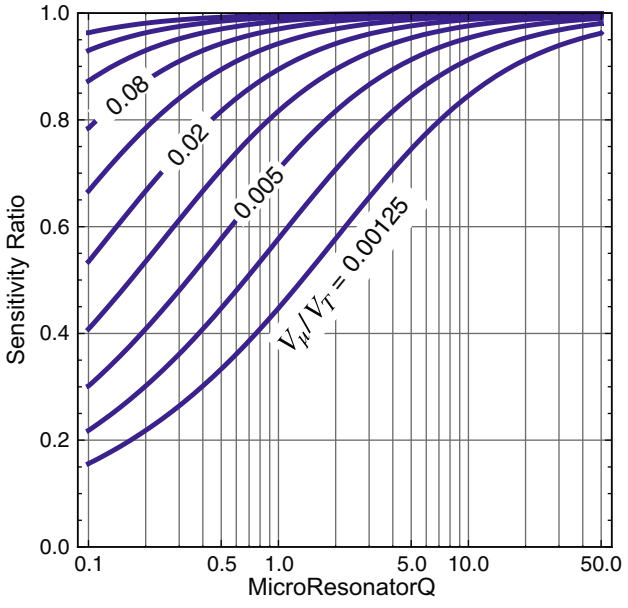

Fig. 4. Ratio of sensitivity of inductively coupled vs direct microcoil NMR, as a function of the quality factor of the microresonator and the volume ratio V_μ/V_T. A probe Q_T of 200 has been assumed. The curves correspond to values of V_μ/V_T from 0.00125 (lowest curve) to 0.64, incremented by factors of 2.

for a volume ratio as small as 0.1%, the sensitivity ratio exceeds 90% for $Q_\mu > 20$. This demonstrates that for typical geometries under consideration in the present context, inductive coupling will lead to a sensitivity loss of only a few percent compared to direct electrical coupling of the microcoil to the NMR receiver circuit. Microcoil Q-factors in this range are quite readily achieved [4–7].

In order to demonstrate that inductively coupled resonators can achieve similar performance to impedance coupled microcoils, the flow profile in a 200μm capillary has been measured using a pulsed field gradient spin echo (PSGE) sequence. As will be shown in the following, the sensitivity is comparable to that reported by Zhang and Webb in a recent study of flow profiles in capillaries of similar dimensions [33].

3. Experimental

All experiments were conducted with a Varian NMR spectrometer, operating at a static field strength of 14.3 T, using a Doty 12 mm microimaging probe. Microresonators were built by winding coils from magnet wire and soldering them to a tunable, non-magnetic capacitor. The microresonators were held in a 12 mm NMR sample tube. Doped water (0.01 M $CuSO_4$, 0.01 M NaCl in H_2O, T_1=350 ms) was used.

4. Results and discussion

In Fig. 1A, a solenoid coil of 10 turns, 1.5 mm inner diameter and 6 mm length has been connected in parallel to a tunable, non-magnetic capacitor, and inserted into a 12 mm NMR tube filled with doped water (0.01 M $CuSO_4$ and 0.05 M NaCl). The dimensions of the coil and the capacitor have been chosen to bring the resonance frequency close to 600 MHz. Fig. 1A shows a sagittal slice obtained with a standard gradient-echo pulse sequence. Only the water inside of the coil contributes noticeably to the signal. The pulse power has been reduced by about 30 dB compared to what would have been necessary to excite the bulk of the sample. The effect of the excitation power on the signal intensity is shown in Fig. 1B. The signal inside the solenoid (circles, a) rises much more rapidly, and to a higher value, than the signal in areas outside (squares, b). The solid lines are fits of the absolute value of a sin function of the square root of the pulse power. For region (a), the maximum signal is obtained at 10 dB, while for region (b), about 35 dB are required.

Fig. 2B shows a Teflon capillary of 0.2 mm inner diameter running through a microcoil of 0.56 mm ID, connected to a tunable capacitor, built into a PMMA support structure. Doped water was circulated through the capillary using a peristaltic pump mounted outside of the magnet bore. The signal strength from the water in the capillary was quantified as a function of the capacitor setting. The capacitance was calibrated externally against the position of the capacitor screw using an impedance meter. For each capacitor setting, the excitation pulse power was varied between −10 and 40 dB. The resulting maximum signal intensity is shown as a function of capacitor setting by the solid circles in Fig. 2C. In addition, the relationship between pulse power and nutation angle was extracted by fitting the intensity data to a sine function. The resulting nutation frequency at 1 W power is also shown in Fig. 2C (open circles).

After appropriate scaling, the maximum intensity as well as the nutation frequency data collapse onto a single curve. This illustrates the validity of the reciprocity principle, which states that the sensitivity is proportional to the magnetic field amplitude generated in the probe volume per unit of current. For the circuit in Fig. 2A, this ratio is given by

$$\frac{B_\mu}{I_T} \propto \frac{\omega k \sqrt{L_\mu L_T}}{\sqrt{R_\mu^2 + (1/\omega C_\mu - \omega L_\mu)^2}}. \quad (9)$$

The solid line in Fig. 2C is a least-squares fit of this expression to the signal intensity data, yielding $L_\mu = 42 \pm 3$nH and $R_\mu = 5.2 \pm 0.5\Omega$. This inductance agrees quite well with that of an ideal solenoid coil of l=2.5 mm length, d=1 mm diameter, and $N = 10$ turns, which is given by $\mu_0 N^2 \pi d^2/4l \approx 39$nH. Together with the observed quality factor of about 24, this value yields $R = 6\Omega$, in very good agreement with the fit value.

The flow velocity profile in the cross section of a circular capillary of 200 μm inner diameter was measured using a spin-echo multi-slice (SEMS) pulse sequence, augmented by a pair of gradient pulses to implement pulsed field gradient spin echo (PGSE) weighting. The microresonator setup shown in Fig. 2A was used for this purpose, with doped water circulated through the capillary by a peristaltic pump. The spin-echo method samples the reciprocal space both in the spatial and the displacement dimension, and yields a data set $S(\mathbf{k},\mathbf{q})$, which must be Fourier-transformed in both dimensions [34]. In the present case, the direction of $\mathbf{q}$ was chosen along the axis of the capillary, and its magnitude was incremented in 40 steps from 0 to $\mathbf{q} = 0.004\mu m^{-1}$. The slice thickness was 200μm.

For each pixel, a displacement profile results after Fourier transformation in the $\mathbf{q}$ dimension. Two such profiles are shown in

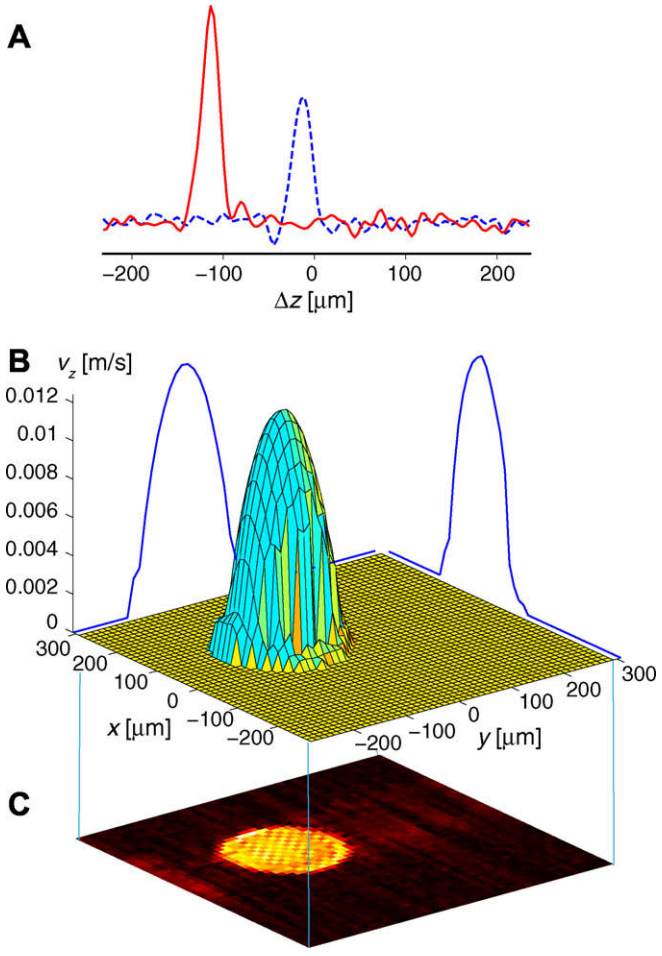

Fig. 5. (Color online) Transport imaging in a PTFE capillary. (A) Displacement profiles from the center (solid line) and the periphery (dashed line) of the capillary. (B) Velocity profile, obtained from the position of the peak in the displacement profile at each pixel. (C) SEMS image of the capillary lumen.

Fig. 5A. The solid and dashed lines correspond to a pixel close to the center and the wall of the capillary, respectively. They indicate the probability $P(\Delta z;\Delta t)$ to find water molecules at position $z+\Delta z$ at time $t+\Delta t$, assuming they were located at z at time t. The delay Δt between the two **q** gradient pulses was fixed at 25 ms in the present work. While the peak width in $P(\Delta z;\Delta t)$ is indicative of the self diffusion coefficient, the flow velocity can be obtained as $v = z_{max}/\Delta t$, where z_{max} is the position of the peak. The flow velocity profile, shown in Fig. 5B, corresponds to the expected parabolic shape. It should be noted that the data represented in Fig. 5 has been acquired in about 2 h of instrument time; this performance is comparable to previous work on similar capillary dimensions carried out with a directly coupled microcoil [33].

As already mentioned, planar, rather than solenoid microcoils are commonly used in microfluidic devices. For example, Massin et al. [5] have demonstrated the fabrication and application of a planar coil of 1 mm diameter with 3 turns, with a self-inductance of $L_\mu = 8.8$nH and a quality factor (at 300 MHz) of $Q_\mu = 18$. A simple calculation shows that inside a solenoid probe coil of $l = 20$mm, $d = 10$mm, and 10 turns, this would give a cross-inductance of $M_\mu = 1.5$nH, or a coupling constant of $k \approx 0.023$. From 8, one finds a value of about 0.8 for the sensitivity ratio. Hence, it is plausible that the inductive coupling approach will work as well with planar microcoils as it is demonstrated here to work with solenoids.

5. Conclusions

Inductively coupled resonators offer a pro-mising way to obtain NMR data from microfluidic systems in a wireless manner. Within certain limits, established in this work, this can be achieved without a substantial sacrifice in sensitivity. Microfluidic devices with integrated resonators could benefit a wide range of applications, including NMR-based diagnostics, metabolomic monitoring [35,36], as well as the study of mixing, chemical reaction, and transport processes. The main challenge lies in the design and efficient microfabrication of integrated planar microcoil resonators with sufficient coupling and *Q*. This work has been supported by the US National Science Foundation (Grant No. DMR-0647790 and CHE-0809795).

References

[1] D.I. Hoult, B. Tomanek, Use of mutually inductive coupling in probe design, Concepts in Magnetic Resonance 15 (2002) 262–285.
[2] M. Bilgen, Inductively-overcoupled coil design for high resolution magnetic resonance imaging, BioMedical Engineering OnLine 5 (2006) 3.
[3] D. Sakellariou, G. Le Goff, J. Jacquinot, High-resolution, high-sensitivity NMR of nanolitre anisotropic samples by coil spinning, Nature 447 (7145) (2007) 694–697.
[4] C. Massin, G. Boero, F. Vincent, J. Abenhaim, P. Besse, R. Popovic, High-Q factor RF planar microcoils for micro-scale NMR spectroscopy, Sensors & Actuators: A. Physical 97 (2002) 280–288.
[5] C. Massin, F. Vincent, A. Homsy, K. Ehrmann, G. Boero, P. Besse, A. Daridon, E. Verpoorte, N. de Rooij, R. Popovic, Planar microcoil-based microfluidic NMR probes, Journal of Magnetic Resonance 164 (2) (2003) 242–255.
[6] H. Wensink, F. Benito-Lopez, D. Hermes, W. Verboom, H. Gardeniers, D. Reinhoudt, A. Berg, Measuring reaction kinetics in a lab-on-a-chip by microcoil NMR, Lab on a Chip 5 (3) (2005) 280–284.
[7] K. Ehrmann, N. Saillen, F. Vincent, M. Stettler, M. Jordan, F. Wurm, P. Besse, R. Popovic, Microfabricated solenoids and Helmholtz coils for NMR spectroscopy of mammalian cells, Lab on a Chip 7 (3) (2007) 373–380.
[8] A. Moule, M. Spence, S. Han, J. Seeley, K. Pierce, S. Saxena, A. Pines, Amplification of xenon NMR and MRI by remote detection, Proceedings of the National Academy of Sciences 100 (16) (2003) 9122–9127.
[9] C. Hilty, E. McDonnell, J. Granwehr, K. Pierce, S. Han, A. Pines, Microfluidic gas-flow profiling using remote-detection NMR, Proceedings of the National Academy of Sciences 102 (42) (2005) 14960–14963.
[10] J. Granwehr, E. Harel, S. Han, S. Garcia, A. Pines, P. Sen, Y. Song, Time-of-Flight Flow Imaging Using NMR Remote Detection, Physical Review Letters 95 (7) (2005) 75503.
[11] F. Bloch, W. Hansen, M.E. Packard, Nuclear induction, Physical Review 69 (1946) 127.
[12] F. Bloch, Nuclear induction, Physical Review 70 (1946) 460.
[13] E.M. Purcell, H.G. Torrey, R.V. Pound, Resonance absorption by nuclear magnetic moments in a solid, Physical Review 69 (1946) 37.
[14] D. Hoult, R. Richards, Critical Factors in the Design of Sensitive High Resolution Nuclear Magnetic Resonance Spectrometers, Proceedings of the Royal Society of London. Series A, Mathematical and Physical Sciences 344 (1638) (1975) 311–340.
[15] D. Hoult, R. Richards, The signal-to-noise ratio of the nuclear magnetic resonance experiment, Journal of Magnetic Resonance 24 (1) (1976) 71–85.
[16] J. Sidles, D. Rugar, Signal-to-noise ratios in inductive and mechanical detection of magnetic resonance, Physical Review Letters 70 (22) (1993) 3506–3509.
[17] D.I. Hoult, Sensitivity of the nmr experiment, in: D. Grant, R. Harris (Eds.), Encyclopedia of NMR, J. Wiley & Sons, Chichester, 1996, pp. 4256–4266.
[18] D. Hoult et al., Sensitivity and power deposition in a high-field imaging experiment, Journal of Magnetic Resonance Imaging 12 (1) (2000) 46–67.
[19] C. Connor, J. Chang, A. Pines, Magnetic resonance spectrometer with a dc SQUID detector, Review of Scientific Instruments 61 (1990) 1059.
[20] D. Rugar, C. Yannoni, J. Sidles, Mechanical detection of magnetic resonance, Nature 360 (6404) (1992) 563–566.
[21] D. Rugar, O. Zuger, S. Hoen, C. Yannoni, H. Vieth, R. Kendrick, Force detection of nuclear magnetic resonance, Science 264 (5165) (1994) 1560–1563.
[22] J. Sidles, J. Garbini, K. Bruland, D. Rugar, O. Züger, S. Hoen, C. Yannoni, Magnetic resonance force microscopy, Reviews of Modern Physics 67 (1) (1995) 249–265.
[23] J. Marohn, P. Carson, J. Hwang, M. Miller, D. Shykind, D. Weitekamp, Optical larmor beat detection of high-resolution nuclear magnetic resonance in a semiconductor heterostructure, Physical Review Letters 75 (7) (1995) 1364–1367.
[24] N. Wu, T. Peck, A. Webb, R. Magin, J. Sweedler, Nanoliter volume sample cells for ^{1}H NMR: application to online detection in capillary electrophoresis, Journal of the American Chemical Society 116 (17) (1994) 7929–7930.
[25] D. Olson, T. Peck, A. Webb, R. Magin, J. Sweedler, High-resolution microcoil ^{1}H NMR for mass-limited, nanoliter-volume samples, Science 270 (5244) (1995) 1967–1970.
[26] K. Minard, R. Wind, Picoliter ^{1}H NMR spectroscopy, Journal of Magnetic Resonance 154 (2) (2002) 336–343.
[27] N. Wu, A. Webb, T. Peck, J. Sweedler, Online NMR detection of amino acids and peptides in microbore LC, Analytical Chemistry 67 (18) (1995) 3101–3107.
[28] R. Subramanian, W. Kelley, P. Floyd, Z. Tan, A. Webb, J. Sweedler, A microcoil NMR probe for coupling microscale HPLC with on-line NMR spectroscopy, Analytical Chemistry 68 (1996) 4431–4435.
[29] A. Wolters, D. Jayawickrama, A. Webb, J. Sweedler, NMR detection with multiple solenoidal microcoils for continuous-flow capillary electrophoresis, Chemical Reviews 99 (1999) 3133–3152.
[30] J. Schewitz, K. Pusecker, P. Gfrörer, U. Götz, L. Tseng, K. Albert, E. Bayer, Direct coupling of capillary electrophoresis and nuclear magnetic resonance spectroscopy for the identification of a dinucleotide, Chromatographia 50 (5) (1999) 333–337.
[31] J. Trumbull, I. Glasgow, D. Beebe, R. Magin, Integrating microfabricated fluidic systems and NMR spectroscopy, Biomedical Engineering, IEEE Transactions on 47 (1) (2000) 3–7.
[32] A. Webb, Nuclear magnetic resonance coupled microseparations, Magnetic Resonance in Chemistry 43 (2005) 688–696.
[33] X. Zhang, A. Webb, Magnetic resonance microimaging and numerical simulations of velocity fields inside enlarged flow cells used for coupled NMR microseparations, Analytical Chemistry 77 (5) (2005) 1338–1344.
[34] P. Callaghan, C. Eccles, Y. Xia, NMR microscopy of dynamic displacements: k-space and q-space imaging, Journal of Physics E: Scientific Instruments 21 (1988) 820–822.
[35] F. Zhang, R. Bruschweiler, Robust Deconvolution of Complex Mixtures by Covariance TOCSY Spectroscopy*, Angewandte Chemie International Ed. 46 (15) (2007) 2639.
[36] D. Snyder, F. Zhang, S. Robinette, L. Bruschweiler-Li, R. Brüschweiler, Non-negative matrix factorization of two-dimensional NMR spectra: application to complex mixture analysis, The Journal of Chemical Physics 128 (2008) 052313.